A Vortex Wake Model for Optimum Heavily Loaded Ducted Fans

ROBIN B. GRAY* AND TERRY WRIGHT†
Georgia Institute of Technology, Atlanta, Ga.

Like the free propeller in axial flight, a single-rotation ducted fan of highest induced efficiency is characterized by an ultimate wake vortex system shed from the blade trailing edges whose apparent motion is that of rigid helical surfaces. In addition and concentric with this inner sheet, there is a cylindrical surface of helical vortex filaments shed from the duct trailing edge. For zero hub diameter, and neglecting compressibility, viscosity, and tip clearance, a consistent mathematical model of the constant-diameter vortex wake is developed and the compatibility relationships to be satisfied are presented. Using the Biot-Savart equation, the vortex strength distribution in the wake may be determined by numerical methods and then related to the blade bound vortex strength. Some preliminary results of the analysis are presented for the lightly loaded case for comparison with existing methods.

Nomenclature

A_1 = coefficient, $A_1 = \cos(\varphi - \varphi_{r_B})$
A_2 = coefficient, $A_2 = \sin(\varphi - \varphi_{r_B})$
b = number of blades
$K(x)$ = nondimensional blade bound vortex distribution, Eq. (25)
M = number of filaments replacing vortex sheet
P = distance from vortex element to control point
r,Ψ,z = cylindrical coordinates
r',Ψ',z' = cylindrical coordinates defining location of vortex filament
r,ξ,ζ = helical coordinates
R = blade tip radius
s' = distance measured along vortex filament
ds' = elemental length of vortex filament
u = disturbance velocity component in direction of subscript
u_{ξ_0} = disturbance velocity component down wake axis
v_i = total disturbance velocity
V_∞ = axial flight velocity
w = apparent axial displacement velocity of blade trailing vortex sheets
w_B = apparent axial displacement velocity of boundary sheet at line of intersection with inner sheets
$\bar{w}$ = nondimensional displacement velocity, $w/\Omega R$
x = nondimensional blade radius
x,y,z = Cartesian coordinates
z'_0 = distance between the $z = 0$ plane and the point where the filament intersects the xz plane
β = angle between the normal to the vectors $d\bar{s}'$ and $\bar{P}$ measured in the plane determined by $d\bar{s}'$ and $\bar{P}$
γ = vortex filament strength
$\gamma(\zeta_B)$ = strength of boundary sheet at its line of intersection with inner sheets
$\Gamma(x)$ = blade bound vortex distribution
λ = tangent of helical pitch angle of inner filaments
λ_B = tangent of helical pitch angle of boundary filaments at their line of intersection with inner sheets
φ = pitch angle of inner filaments
φ_B = pitch angle of boundary filaments at their line of intersection with inner sheets
φ_{rB} = dummy helical pitch angle related to φ_B
φ_R = pitch angle of outermost filament of inner sheets
Ω = blade rotational velocity

Subscripts

B = line of intersection of inner helical sheets with boundary sheet
m = vortex filament
R = outermost filament of helical inner sheets

Presented as Paper 69-222 at the AIAA/AHS VTOL Research, Design, and Operations Meeting, Georgia Institute of Technology, Atlanta, Ga., Feb. 17–19, 1969. Submitted March 6, 1969; revision received July 25, 1969. This work is supported by the U.S. Army Research Office-Durham under Contract No. DAHC04 68 C 0004.

* Professor, School of Aerospace Engineering. Member AIAA.
† Graduate Research Assistant, School of Aerospace Engineering.

Introduction

IT has been shown by Betz[1] that an isolated propeller in axial flight having the highest possible induced efficiency generates an ultimate wake vortex system which moves through the fluid medium as if the vortex sheets of the wake were rigid helical surfaces of constant pitch. Determination of the required radial distribution of the vortex sheet strength associated with this motion is relatively straightforward and has been done by Goldstein[2] and Theodorsen.[3]

For the optimum ducted fan in axial flight, the same considerations and arguments hold concerning the geometry and motion of the helical vortex sheets which are shed from the blade trailing edges. The geometric pitch of each filament of these sheets must be constant and the sheets must appear to move as rigid screw surfaces. There is, however, the additional constraint that the Kutta condition must be satisfied at the duct trailing edge. Thus, if the flow at the duct trailing edge is to be tangent to the mean camber surface, a sheet of vorticity must be shed from the duct trailing edge forming a boundary sheet of helical vortex filaments enclosing the screw-like sheets shed from the blades. If the wake has reached its ultimate configuration at the duct trailing edge then the boundary vortex sheet is composed of filaments wrapped on a right circular cylinder. For the lightly loaded ducted fan, the geometric pitch of both systems is the same and this case has been solved by Tachmindji,[4] Theodorsen,[5] and Gray.[6,7] For the heavily loaded case, the inner vortex sheets must move at a different rate from that of the boundary sheet. It is the description of this relative motion and the development of the necessary compatibility relationships that form the major part of this paper. The actual design data and the performance equations will be presented in a subsequent paper.

In recent years, Morgan,[8] Ordway, Sluyter, and Sonnerup,[9] Chaplin,[10] and others have published papers in the field of ducted fans with primary emphasis on the shroud design. The results of the analysis of this paper will complement

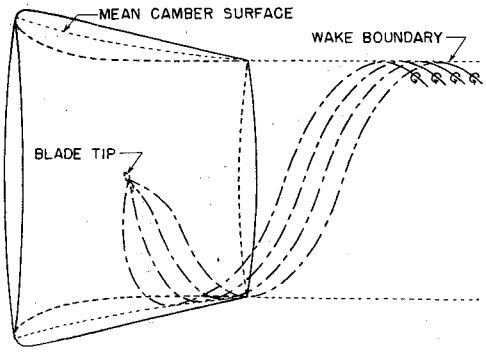

Fig. 1 Conceptual diagram of the continuation of the blade bound vortex onto the duct mean camber surface and subsequent shedding at the duct trailing edge.

these papers by providing a blade bound vortex strength distribution for the heavily loaded fan.

The effects of hub diameter, compressibility, viscosity, and tip clearance are neglected in the analysis. The results will therefore give an upper limit on the performance of single-rotation fans without stator vanes for comparison with other design methods. The effect of compressibility on the wake analysis should be small as long as the disturbance velocity Mach number is below approximately 0.3. The amount of tip clearance and the interaction of the tip with the shroud boundary layer will have an effect on the predicted performance. Tip clearance has been accounted for in several papers[4,8,9] for the lightly loaded case. At present, a satisfactory model for the heavily loaded propeller with tip clearance has not been devised.

Model of Wake Vortex System

The argument concerning the geometry and motion of the ultimate wake vortex system of an optimum single-rotation ducted fan is essentially the same as that presented by Theodorsen[3] for the free propeller. Thus, in Ref. 6, it is shown that the optimum condition is obtained for the ducted fan when the helical vortex sheets shed from the blades appear to move as rigid screw surfaces in the ultimate wake. This is identical with the requirement of the free propeller. The principal difference between the two arguments is that for the heavily loaded ducted fan case, the disturbance velocity vector is not normal to the vortex sheet surface. No other information is obtained about the geometry and other relationships must be developed in order to assure a compatible vortex model.

Additional information may be obtained through a consideration of the flowfields associated with the vortex systems. The blade trailing vortex system has large radial velocity components associated with it and, with respect to a reference system fixed in the duct, this flow is periodic. If the duct mean camber surface is to correspond to a streamline, a distribution of vorticity must be placed along this surface to cancel all normal velocity components. Part of this distribution must also be periodic in nature and must be a function of the number of blades in the propeller or fan. That is, it must rotate with the blades. A portion of this periodic distribution is considered to be a continuation of each blade bound vortex which passes directly from the blade tip onto the duct contour where it spreads out over the duct mean camber surface. Then in accordance with the Helmoltz theorems, it moves aft along the mean camber surface and is shed at the duct trailing edge as free helical vortex filaments of varying density wrapped on a cylindrical surface. While these filaments are within the contour it is assumed that they make all of the necessary adjustments in phase relationship with the blade trailing vortex system so that the motion of this wake boundary system is along the tangent to the mean camber surface at the trailing

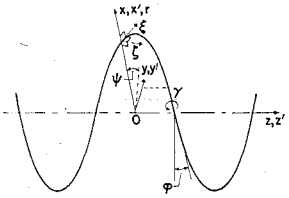

Fig. 2 Helical coordinate system.

edge of the shroud as shown in Fig. 1. This in effect satisfies the Kutta condition. The remaining portion of the periodic duct vortex distribution is considered to be bound to the duct and to rotate with the blades. It does not contribute to the wake vortex system. It is also assumed that the duct is designed so that there is no contraction or expansion of the wake downstream of the fan. This is a feasible design problem[10] and guarantees that the duct is compatible with the wake geometry of the analysis.

Wakes having an initial expansion or contraction[10] may be considered if it is assumed that a given vortex filament remains at the same nondimensional radial position as it progresses down the wake. This complicates the analysis as continuity and a force-free vortex wake must be maintained while physical limitations such as flow separations must be avoided. Design of the fan blades also depends upon the geometry of the expanding or contracting wake and proceeding from the ultimate wake to the blade position for design purposes becomes more involved. The integrity of the rigid ultimate wake vortex system must also be undisturbed by the initial distortions. Therefore, even though an expanding wake may yield a higher figure of merit, the additional complexities introduced become more difficult to handle. Thus, the term optimum as used in this paper refers to a fan or propeller of highest induced efficiency for the assumed wake geometry. Profile drag losses and tip effects will reduce the efficiency and the final result will depend upon the experience of the designer in keeping these effects to a near minimum.

Consider a helical coordinate system r, ξ, ζ defined in terms of the cylindrical coordinates r, Ψ, z as shown in Fig. 2, so that at a given instant an inner helical vortex sheet in the ultimate wake coincides with the $\zeta = 0$ surface. Then

$$r = r, \quad 0 \leq r \leq \infty \tag{1}$$

$$\xi = r\Psi \cos\varphi + z \sin\varphi, \quad -\infty \leq \xi \leq \infty \tag{2}$$

$$\zeta = -r\Psi \sin\varphi + z \cos\varphi, \quad -\frac{(V_\infty + w)\cos\varphi}{2b(\Omega/2\pi)} \leq \zeta \leq \frac{(V_\infty + w)\cos\varphi}{2b(\Omega/2\pi)} \tag{3}$$

The uniform apparent motion of the inner sheets requires helical symmetry of the boundary vortex sheet strength distribution with respect to the intersection of the inner sheets with the boundary sheets for zero radial velocities at the inner sheets. Therefore the disturbance velocity vector will be constant along helical lines $r = \text{const}$, $\zeta = \text{const}$ both inside and outside the ultimate wake. Consider the line integral of the velocity along the path $\overline{ABCDA}$ within the wake as shown in Fig. 3. The velocity diagram with respect to the rotating blades is showing in Fig. 4. Along $\overline{BC}$, u_ξ is constant since r and ζ are constant. $\overline{AB}$ and $\overline{CD}$ are radial lines intersecting

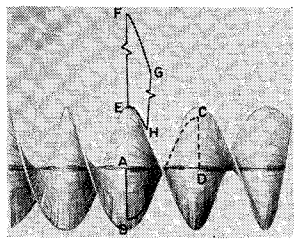

Fig. 3 Ultimate wake system showing the paths along which the line integrals are evaluated.

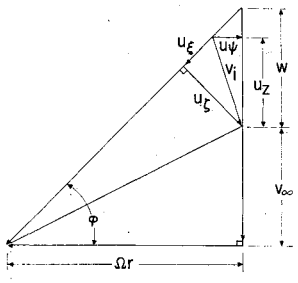

Fig. 4 Velocity diagram with respect to the rotating blades at an inner helical vortex filament of the ultimate wake.

the same helical coordinate lines and $\overline{DA}$ coincides with the wake axis. The path so described lies on the surface of a helical vortex sheet. No vorticity is enclosed by this path so that the line integral must be zero. Thus,

$$\int_A^B u_r dr + \int_B^C u_\xi \, d\xi + \int_C^D u_r dr + \int_D^A u_\xi \, d\xi = 0$$

Since

$$u_r\Big|_{\overline{AB}} = u_r\Big|_{\overline{DC}}, \quad u_\xi (\xi_C - \xi_B) + u_{\xi_0} (z_A - z_D) = 0$$

or

$$- u_\xi \left\{ r \frac{2\pi}{b} \cos\varphi + \frac{V_\infty + w}{b(\Omega/2\pi)} \sin\varphi \right\} + u_{\xi_0} \frac{V_\infty + w}{b(\Omega/2\pi)} = 0$$

so that from Fig. 4 $u_\xi = u_{\xi_0} \sin\varphi$.

A similar line integral along the path $\overline{EFGHE}$ establishes the same result outside of the ultimate wake. Further, since for the helical coordinate ζ

$$\tan \varphi = (R/r) \tan\varphi_R \tag{4}$$

φ approaches zero as r approaches infinity so that u_ξ becomes zero as r becomes infinite.

These results are subject to the additional condition that the line integral of the velocity along a path enclosing the wake must be zero to obtain a single-valued solution outside of the wake. The line integral is taken along the path $\overline{ABCA}$ in Fig. 5 where u_ξ is constant along $\overline{ABC}$ so that

$$\int_C^A u_z \, dz + 2\pi R u_{\xi_0} \tan \varphi_R = 0$$

The integral is then taken along $\overline{ACDEA}$. Subject to helical symmetry, the induced velocity is zero along the radial lines $\overline{CD}$ and $\overline{EA}$. If $\overline{DE}$ is allowed to approach infinity then u_z along $\overline{DE}$ is zero. Since no vorticity is enclosed by the path,

$$\int_C^A u_z \, dz = 0$$

Therefore, the line integral along the closed path $\overline{ABCA}$ is zero for a helically symmetrical system having all filaments at the same geometric pitch only if $u_{\xi_0} = 0$. That is, for an ultimate wake vortex system in which no relative axial motion occurs between the inner and outer systems, u_{ξ_0} must be zero in order to obtain a solution for which the flow outside of the wake is irrotational. This is the lightly loaded case considered in Refs. 6 and 7 for which the disturbance velocity is normal to the inner sheets.

For the heavily loaded system for which u_{ξ_0} is not zero, a geometry and motion must be established which will maintain the helical symmetry of vortex strength distribution on the boundary, will permit the boundary sheet filaments of the ultimate wake to have an axial motion relative to the inner sheets, and will result in no disturbance velocities outside of the constant diameter wake. The first stipulation guarantees that there will be no radial disturbance velocities at the inner filaments due to the boundary filaments. The second is a consequence of the heavily loaded condition. The third is the necessary requirement for irrotational flow outside of the wake as shown in the following discussion.

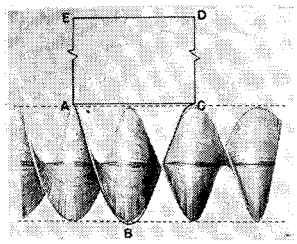

Fig. 5 Ultimate wake vortex system showing paths along which the line integrals are evaluated.

Any flowfield associated with a system of vortex filaments satisfies continuity everywhere and is irrotational everywhere except at the filaments themselves. According to Helmholtz' second theorem, the summation of the shed vorticity must be zero. Hence the line integral of the disturbance velocities along any path enclosing the wake and any closed path outside of the wake must be zero. Considering the line integral of the velocities along the closed path $\overline{ABCDEA}$ in Fig. 5, the line integral of u_ξ along $\overline{ABC}$ must be zero since u_r is zero along $\overline{CD}$ and $\overline{EA}$ and u_z is zero along $\overline{DE}$. Because of the helical symmetry, the direction of u_ξ cannot change with respect to the direction of integration so that u_ξ must also be zero. By fixing the path $\overline{CDEA}$, moving the helical line $\overline{ABC}$ axially to points designated A′, B′, C′, and closing the path by axial line segments $\overline{AA'}$, $\overline{C'C}$ which have equal but opposite u_z contributions, it may be easily shown that u_ξ must be zero everywhere outside the wake.

If it is assumed that u_r and u_z are not zero everywhere outside of the wake, then in order for the line integral of u_z along $\overline{AC}$ to be zero, u_z must change direction with respect to this path and flow cells exist in the external flow. Vortex flows satisfy continuity everywhere so that it is possible to construct the streamlines in these cells. These streamlines can only be closed and the line integral of the velocity along any one of these streamlines within the cell will be different from zero. Hence the flow is rotational in these regions, which violates Helmholtz' third theorem. The conclusion is that for the constant diameter wake, the only possible irrotational flow satisfying continuity in the external region is one in which all of the disturbance velocities are zero. Thus, when the boundary conditions on the wake are satisfied by the proper vortex strength distributions, the velocities outside the wake are automatically zero.

In cases where the velocity fields associated with the vortex sheets of the ultimate wake can be obtained by explicit integration of the Biot-Savart relation, the result is the same: that is, all induced velocities are zero outside of the wake. Examples of such a case are ducted propellers with an infinite number of blades having either a constant blade circulation or an optimum heavily loaded blade circulation.

On the inner sheets, the condition of u_ξ still applies and, for rigid motion of the inner sheet, u_ζ must be proportional to

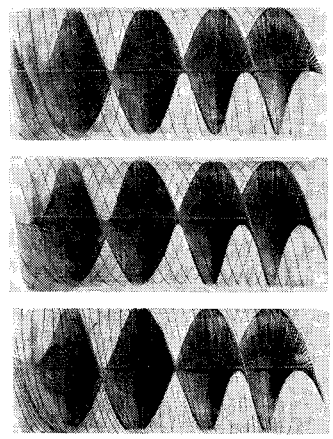

a) Boundary sheet of uniform strength and constant helix pitch angle φ_B

b) Boundary sheet of varying strength and constant helix pitch angle φ_R

c) Result of superposition of the two boundary sheets

Fig. 6 Concept of ultimate wake vortex system.

$\cos\varphi$. That is, from the previous results and the velocity diagram of Fig. 4

$$u_\xi = u_{\xi_0} \sin\varphi \tag{5}$$

and

$$u_\zeta = w \cos\varphi \tag{6}$$

For the last outboard filament of each inner sheet in the ultimate wake (at $r = R$) $u_{\xi_R} = u_{\xi_0} \sin\varphi_R$, $u_{\zeta_R} = w \cos\varphi_R$. The filaments in the boundary sheet that are adjacent to this last outboard filament must have a velocity normal to their helical coordinate of

$$u_{\zeta_B} = \tfrac{1}{2}(u_{\xi_0}^2 \sin^2\varphi_R + w^2 \cos^2\varphi_R)^{1/2} \tag{7}$$

and the boundary sheet strength at this point in the ultimate wake must be

$$\gamma(\zeta_B) = (u_{\xi_0}^2 \sin^2\varphi_R + w^2 \cos^2\varphi_R)^{1/2} \tag{8}$$

in order to limit the disturbance velocities to the inside of the wake and to assure irrotationality outside of the wake. These two relationships are obtained directly from the conditions that the disturbance velocities are zero outside of the wake, that the strength of a vortex sheet is equal to the discontinuity in the velocity components as the sheet is crossed, and that the motion of the sheet along the line of discontinuity is equal to the mean value of the velocity on either side.

Therefore, the helical boundary vortex filaments must all cross the lines of intersection between the inner screw surfaces and the boundary sheet at a constant angle φ_B not equal to φ_R. This angle may be determined from the flight speed, the blade rotational velocity, and the total disturbance velocity of Eq. (7). The boundary sheet strength must also be constant along the lines of intersection and equal to the result of Eq. (8). Thus, when relative motion exists between the inner sheets and the boundary filaments, the two vortex systems are related through Eqs. (7) and (8) but only along the lines of intersection. On the wake boundary between the helical lines of intersection, the filament density or sheet strength and the filament pitch angle must vary with the helical coordinate ζ.

The boundary vortex sheet primarily serves three purposes. First, it must cancel the radial velocity field associated with the rigid inner screw surfaces at the boundary. Second, it must accommodate the discontinuity in velocity as the boundary is crossed. Third, it must not disturb the apparent rigid motion of the inner sheet, i.e., it must not induce radial velocities at the inner sheet. The first and second conditions are satisfied by the sheet strength distribution and the filament geometry, both as yet unknown. The third condition may be automatically satisfied by a strength distribution and geometry that are symmetrical about the lines of intersection as noted before.

Having to solve for both the strength distribution and the geometry presents additional difficulties which may be eliminated by replacing the boundary sheet by two simpler systems whose combined effect does not change the inner flowfield. The first of these is a uniform sheet of helical vortex filaments having constant density $\gamma(\zeta_B)$ and constant helix pitch angle φ_B as shown in Fig. 6a. The second is a cylindrical sheet of helical filaments of varying and unknown strength but having the constant and known helix pitch angle φ_R as shown in Fig. 6b. The first sheet satisfies the required conditions along the lines of intersection as previously discussed. The second sheet has zero strength at the lines of intersection, has a symmetrical strength distribution about these lines and the midpoint between the lines of intersection, and cancels the radial velocities at the boundaries. Superposition of the two sheets as shown in Fig. 6c must maintain the apparent rigid motion of the inner screw surface. This is the condition that will be placed on the solution.

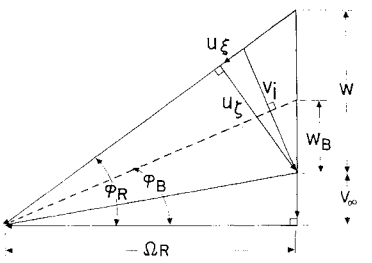

Fig. 7 Velocity diagram with respect to the rotating blades of the outermost filament of the inner vortex sheet and at the adjacent point of the boundary sheet in the ultimate wake.

It should be noted that, to an observer fixed on an inner helical sheet, the boundary vortex sheet (consisting of the superposition of the two simpler sheets) appears in terms of the local strength distribution to be fixed relative to the inner sheet. Although the boundary sheet is actually slipping upward relative to the inner sheets, the observer sees the same local vortex strength at a given point on the boundary at any instant of time, but the identity of the filaments at the point is constantly changing.

Now consider the geometry and motion of the uniform sheet relative to the last outboard filament of an adjacent inner helical vortex sheet. The velocity diagram with respect to the rotating blades as shown in Fig. 7 illustrates the relationship between the velocities associated with the two systems according to the compatibility conditions previously expressed. Thus, from Fig. 7,

$$\lambda = \tan\varphi_R = (V_\infty + w)/\Omega R \tag{9}$$

$$\lambda_B = \tan\varphi_B = (V_\infty + w_B)/\Omega R \tag{10}$$

where

$$w_B = \tfrac{1}{2}(u_{\xi_0}^2 \sin^2\varphi_R + w^2 \cos^2\varphi_R)^{1/2} \sec\varphi_B \tag{11}$$

From this same figure,

$$u_{\xi_0} \sin\varphi_R / w \cos\varphi_R = \tan(\varphi_R - \varphi_B) \tag{12}$$

Combining Eqs. (11) and (12) to eliminate u_{ξ_0} and substituting for the trigonometric functions of Eqs. (9) and (10) yields

$$\lambda_B = \lambda - \bar{w}\{1 - [\tfrac{1}{2}(1 + \lambda_B^2)/(1 + \lambda\lambda_B)]\}$$

where $\bar{w} = w/\Omega R$. This result shows that, for any choice of λ and $\bar{w}$, λ_B can be determined uniquely. It should be noted that for vanishingly small values of $\bar{w}$, λ_B approaches λ, which is in agreement with the lightly loaded case. Further, there would seem to be no simple redefinition of λ which would reduce the solutions to a single case for all values of $\bar{w}$. This is in agreement with the earlier analysis of Ref. 6.

Solving this last expression for the tangent of the helix pitch angle of the boundary filaments at the line of intersection yields

$$\lambda_B = \lambda - \frac{\lambda^2 + 1}{2\lambda - \bar{w}} + \left\{\left(\lambda - \frac{\lambda^2 + 1}{2\lambda - \bar{w}}\right)^2 + 1\right\}^{1/2} \tag{13}$$

Since $\varphi_B = \tan^{-1}\lambda_B$, the value of $\gamma(\zeta_B)$ is known according to

$$\gamma(\zeta_B) = w \cos\varphi_R \sec(\varphi_R - \varphi_B) \tag{14}$$

The compatibility condition at the boundary automatically assures a continuous static pressure variation throughout the flow in the ultimate wake. This may be seen from Fig. 7 in which the velocity magnitude is the same both immediately inside and outside of the wake boundary. Note that the resultant velocity diagram having v_i as its base is geometrically an isosceles triangle. Thus, the steady Bernouli's equation may be written in the rotating system and the static pressure is the same inside and outside the boundary and is identically equal to the freestream static pressure. Therefore, the vortex wake is a force-free system.

The ultimate wake vortex system of the heavily loaded ducted fan is thus defined in terms of the inner helical sheets of Fig. 5 (one for each blade), a vortex sheet of uniform

strength $\gamma(\zeta_B)$ and constant filament pitch angle φ_B lying on the cylindrical wake boundary as shown in Fig. 6a, and a sheet of varying strength but constant filament pitch angle φ_R also lying on the cylindrical wake boundary as in Fig. 6b. For a given b, λ, and $\bar{w}$, the geometry and motion of the system are determined along with the strength of the uniform boundary sheet. The solution for the strength distribution of the inner helical sheets, and thus for the blade bound vortex strength, proceeds directly from the numerical integration of the Biot-Savart equation for the velocity at certain control points that is associated with each vortex filament in the wake.

Analysis

From the discussion of the preceding section, the geometry and motion of the ultimate wake vortex system of infinite length are known. The problem is now to find the distribution of vorticity in the wake which will satisfy the boundary conditions implied by this geometry and motion. In this analysis, the Biot-Savart equation supplies the required relationship between the geometry, motion, and vortex sheet strengths. Thus, for an elemental length of an arbitrary vortex filament,

$$dv_i = \gamma \cos\beta ds'/4\pi P^2 \tag{15}$$

The integral relations for the velocity components in Cartesian coordinates are given by Lamb.[11] However, the boundary conditions are more conveniently expressed in terms of the velocity components along and perpendicular to the vortex filaments. These helical components are obtained from the Cartesian components as follows:

$$u_r = u_x \cos\Psi + u_y \sin\Psi$$

$$u_\xi = (u_y \cos\Psi - u_x \sin\Psi)\cos\varphi + u_z \sin\varphi$$

$$u_\zeta = u_z \cos\varphi - (u_y \cos\Psi - u_x \sin\Psi)\sin\varphi$$

Then replacing the vortex sheet by a number of finite strength vortex filaments, and employing the helical relation, $r \tan\varphi = r' \tan\varphi' = R \tan\varphi_R$, the elemental velocity components associated with one filament become

$$\frac{\Delta u_r}{w} = \frac{\gamma}{4\pi R w}\int_{-\infty}^{\infty} \{\bar{r}' \tan\varphi_R \sin(\Psi' - \Psi) + \bar{r}'[\bar{z} - \bar{z}_0' - \Psi' \tan\varphi_R]\cos(\Psi' - \Psi)\}\frac{d\Psi'}{\bar{P}^3} \tag{16}$$

$$\frac{\Delta u_\xi}{w} = \frac{\gamma \cos\varphi}{4\pi R w}\int_{-\infty}^{\infty} \left\{\bar{r}'\left[\tan\varphi_R\left(\frac{\bar{r}'}{\bar{r}} + \frac{\bar{r}}{\bar{r}'} - 2\cos(\Psi' - \Psi)\right) + [\bar{z} - \bar{z}_0' - \Psi' \tan\varphi_R]\sin(\Psi' - \Psi)\right\}\frac{d\Psi'}{\bar{P}^3} \tag{17}$$

$$\frac{\Delta u_\zeta}{w} = \frac{\gamma \cos\varphi}{4\pi R w}\int_{-\infty}^{\infty} \left\{\bar{r}'^2 - \bar{r}\bar{r}'\cos(\Psi' - \Psi) - \tan^2\varphi_R\left[1 - \frac{\bar{r}'}{\bar{r}}\cos(\Psi' - \Psi)\right] - \frac{\bar{r}'}{\bar{r}}\sin(\Psi' - \Psi)\tan\varphi_R[\bar{z} - \bar{z}_0' - \Psi' \tan\varphi_R]\right\}\frac{d\Psi'}{\bar{P}^3} \tag{18}$$

where

$$\bar{P}^2 = \bar{r}^2 + \bar{r}'^2 - 2\bar{r}\bar{r}'\cos(\Psi' - \Psi) + [\bar{z} - \bar{z}_0' - \Psi' \tan\varphi_R]^2$$

$$\varphi = \tan^{-1}[(1/\bar{r})\tan\varphi_R]$$

and $\bar{r}$, $\bar{r}'$, $\bar{z}$, $\bar{z}_0'$ are nondimensionalized by R.

The boundary conditions to be satisfied by the system are as follows:

on the inner sheet:

$$\sum\left(\frac{\Delta u_\zeta}{w}\right) = \cos\varphi \tag{19}$$

$$\sum\left(\frac{\Delta u_r}{w}\right) = 0 \tag{20}$$

on the cylindrical boundary:

$$\sum\left(\frac{\Delta u_r}{w}\right) = 0 \tag{21}$$

The uniform boundary sheet induces velocities only in its ξ and ζ directions. The nonuniform boundary sheet has symmetrical strength distributions above and below its line of intersection with the inner sheets so that it induces no radial velocities at the inner sheet. Examination of the integrand of Eq. (16) reveals that no radial velocities are induced on the inner sheet by the sheet itself. Thus, Eq. (20) is satisfied identically. The condition on the cylindrical boundary, Eq. (21), involves only the inner sheets and the nonuniform boundary sheet. The condition given by Eq. (19) on the inner sheet involves all three vortex sheets. An additional constraint necessary to obtain a unique solution is that the sum of the strengths of all of the vortex filaments comprising the system be zero.

The boundary conditions now become

on the inner sheet:

$$\sum_1\left(\frac{u_\zeta}{w}\right) + \sum_2\left(\frac{u_\zeta}{w}\right)A_1 - \sum_2\left(\frac{u_\xi}{w}\right)A_2 + \sum_3\left(\frac{u_\zeta}{w}\right) = \cos\varphi \tag{22}$$

on the cylindrical boundary:

$$\sum_1\left(\frac{u_r}{w}\right) + \sum_3\left(\frac{u_r}{w}\right) = 0 \tag{23}$$

and

$$\sum_1\left(\frac{\gamma}{4\pi R w}\right) + \sum_2\left(\frac{\gamma}{4\pi R w}\right) + \sum_3\left(\frac{\gamma}{4\pi R w}\right) = 0 \tag{24}$$

where

$\sum_1$ is over the filaments of the inner sheets,

$\sum_2$ is over the filaments of the uniform boundary sheet,

$\sum_3$ is over the filaments of the nonuniform boundary sheet;

$$A_1 = \cos(\varphi - \varphi_{r_B}),\ A_2 = \sin(\varphi - \varphi_{r_B}),$$

$$\tan\varphi = (1/\bar{r})\tan\varphi_R,\ \tan\varphi_{r_B} = (1/\bar{r})\tan\varphi_B.$$

Preliminary Results

The integrations required to generate the velocity component contributions of a helical vortex filament have been programed for the digital computer. Initial calculations have been made for the limiting case of a single turn of the helix at zero helix pitch angle for comparison to ring vortex results. This comparison was satisfactory and the calculations were then extended to obtain the velocity contributions of a full helical vortex filament which is the basic element of the vortex system to be considered. Provision was made for an internal determination of the angular interval of numerical integration

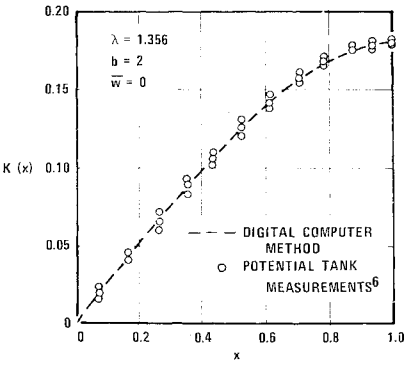

Fig. 8 A comparison of two methods of determining the blade bound vortex strength distribution function for a lightly loaded ducted propeller.

required for a specified degree of accuracy and for the permissible truncation of the infinite length of the filament.

Free Propeller

Following these initial efforts, the various velocity-component calculation procedures were combined into a single program including a procedure for the solution of a system of linear algebraic equations. This program was set up to generate the velocity component coefficients in terms of unknown vortex filament strengths for control points along a radius of the helical inner sheet in the ultimate wake. The sheet was divided into M strips of equal width and the strips were replaced by filaments of finite but unknown strength lying along the centerline of each strip. $(M - 1)$ control points were placed midway between adjacent filaments. The normal component of the disturbance velocity of each control point of the sheet for each filament was then calculated, summed, and set equal to the required normal velocity at each point as given by Eq. (19). The result was an $(M - 1)$ by M system of linear equations in M unknowns with the Mth equation provided by the zero net vorticity requirement of Eq. (24).

The calculations were performed and the system was solved successively for $M = 4$, 6, 8, 10, 12, and 18 filaments with $\lambda = \frac{1}{2}$ and $b = 2$. The results were compared with those of Goldstein[2] in order to determine the degree of error associated with the approximation of a vortex sheet by a finite number of filaments and to determine the effect of the numerical integration parameters on the accuracy of the solution. These results indicated that for ten filaments, the difference incurred was about 2%. Larger numbers of filaments reduced this difference rather slowly and the improvement does not seem to justify the larger computation time involved. Variation of the numerical integration intervals showed that adequate smoothness and accuracy of the solution were obtained when the angular segment was of the order of two degrees and the contribution of the final turn of the helical filament to the velocity coefficient was of the order of 2%.

Lightly Loaded Ducted Fan

The system for the solution of the heavily loaded ducted fan, as outlined earlier, was then set up in a form which would permit the solution of the limit case of a vanishing loading. Utilizing the results of the free propeller study, the system was solved for ten filaments on the helical inner sheets and for eight filaments on the nonuniform boundary sheet. It was necessary at this point to resort to a Fourier series representation for the sheet strength distribution in order to assure the required symmetry on the boundary and to force the nonuniform sheet strength to be zero at the lines of intersection with the helical inner sheets.

Solutions were generated for comparison with the electropotential analogy results of Ref. 6. The results of $\lambda = 1.356$ and $b = 2$ are shown in Fig. 8. $K(x)$ is the nondimensional

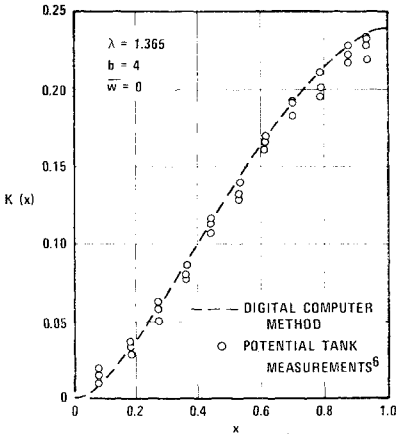

Fig. 9 A comparison of two methods of determining the blade bound vortex strength distribution function for a lightly loaded ducted propeller.

blade bound vortex strength distribution defined as

$$K(x) \equiv b\Gamma(x)/2\pi Rw\lambda \tag{25}$$

where x is the nondimensional radius and $\Gamma(x)$ is the sum of the filament strengths shed inboard of x. The same comparison for a four-bladed propeller is shown in Fig. 9. In both cases the comparison is considered to be good.

Solutions were also generated for comparison with the theoretical results of Tachmindji[4] who used the velocity potential approach. The comparison was again considered to be good.

In addition, the system was calculated and solved for different numbers of blades (from 2–24) in order to observe the rate of convergence to the explicit solution for the lightly loaded ducted propeller with an infinite number of blades as given by Theodorsen.[3] The results are shown in Fig. 10 for the blade bound vortex strength distribution. Although there are no other data for comparison purposes, the results appear to be reasonable.

Concluding Remarks

On the basis of these results and comparisons, it appears that the numerical procedures employed for replacing the

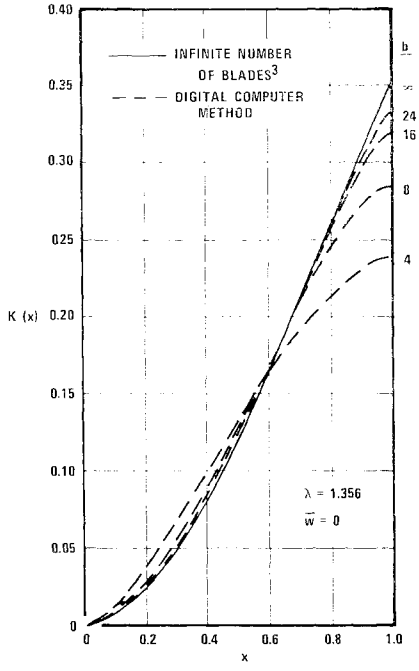

Fig. 10 A comparison of the blade bound vortex strength distribution function for a lightly loaded ducted propeller for successive numbers of blades (digital computer solution) with the infinite blade solution (exact).

vortex system of a ducted fan with a number of finite strength vortex filaments are satisfactory. Therefore, the light-loading restriction has been removed and investigation of the heavily loaded system has begun. The design data and performance equation will appear in a later paper.

References

[1] Betz, A., "Schraubenpropeller mit geringstem Energieverlust," Nachrichten von der Gesellschaft der Wissenschaften zu Göttingen, Mathematisch-Physikalische Klasse, Heft 2, 1919, pp. 193–217.

[2] Goldstein, S., "On the Vortex Theory of Screw Propellers," *Proceedings of the Royal Society (London), Ser. A*, Vol. 112, No. 792, 1929, pp. 440–465.

[3] Theodorsen, T., *Theory of Propellers*, McGraw-Hill, New York, 1948.

[4] Tachmindji, A. J., "The Potential Problem of the Optimum Propeller with Finite Number of Blades Operating in a Cylindrical Duct," Rept. 1228, July 1958, David Taylor Model Basin, Washington, D. C.

[5] Theodorsen, T., "Theoretical Investigation of Ducted Propeller Aerodynamics," Vol. III, TCREC TR 61-119, Sept. 1961, U.S. Army Transportation Research Command, Fort Eustis, Va.

[6] Gray, R. B., "An Investigation of an Approach to the Problem of Determining the Optimum Design of Shrouded Propellers," TCREC 60-44, May 1960, U.S. Army Transportation Research Command, Fort Eustis, Va.

[7] Gray, R. B., "An Investigation of a Digital Computer Method of Determining the Optimum Design Parameter of Shrouded Propellers," TCREC TR 61-124, Oct. 1961, U.S. Army Transportation Research. Command, Fort Eustis, Va.

[8] Morgan, W. B., "Theory of the Annular Airfoil and Ducted Propeller," *Fourth Symposium on Naval Hydrodynamics* ONR, ACR-73, Vol. I, Dept. of the Navy, Washington, D.C., pp. 161–212.

[9] Ordway, D. E., Sluyter, M. M., and Sonnerup, B. O. U., "Three-Dimensional Theory of Ducted Propellers," TAR-TR 602, Aug. 1960, Therm Advanced Research Division of Therm Corp., Ithaca, N.Y.

[10] Chaplin, H. R., "A Method for Numerical Calculation of Slipstream Contraction of a Shrouded Impulse Disc in the Static Case with Application to Other Axisymmetric Potential Flow Problems," Rept. 1857, June 1964, David Taylor Model Basin, Washington, D.C.

[11] Lamb, H., *Hydrodynamics*, Dover, New York, 1945.